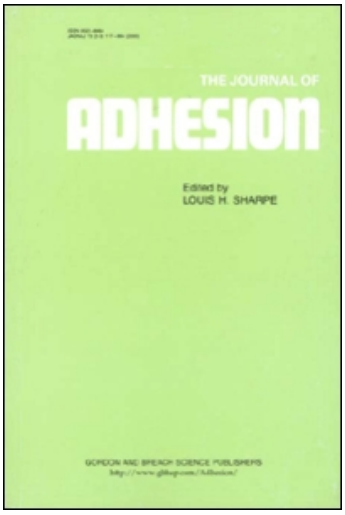

The Journal of Adhesion
Publication details, including instructions for authors and subscription information:
http://www.informaworld.com/smpp/title~content=t713453635

Graphite Fibre-Epoxy Matrix Interface Interactions

H. M. Hawthorne[a]; E. Teghtsoonian[a]
[a] Centre for Materials Research, University of British Columbia, Vancouver, B.C., Canada

To cite this Article Hawthorne, H. M. and Teghtsoonian, E.(1974) 'Graphite Fibre-Epoxy Matrix Interface Interactions', The Journal of Adhesion, 6: 1, 85 — 105
To link to this Article: DOI: 10.1080/00218467408072239
URL: http://dx.doi.org/10.1080/00218467408072239

J. Adhesion, 1974, Vol. 6, pp. 85–105

Printed in Northern Ireland

Graphite Fibre—Epoxy Matrix Interface Interactions†

H. M. HAWTHORNE and E. TEGHTSOONIAN

Centre for Materials Research, University of British Columbia, Vancouver, B.C., Canada

(*Received June 18, 1973*)

Studies of fibre-epoxy resin matrix model composites show that the "tensile debond" test is not applicable to carbon or graphite fibres. Fibre fracture occurs under the compression strains involved relieving interface stresses and precluding subsequent debond. Calculated minimum bond strengths for pitch-based graphite fibres are similar to results for boron and glass fibres. Interfacial failure is obtained with the "shear debond" test for low and intermediate modulus graphite fibres, but compression fracture also occurs first with high modulus fibres. Pitch-based graphite fibres show a decreasing adhesive interaction with epoxy resin the more oriented the fibre, but results compare favorably with those of other fibres. Surface characterisation shows that all pitch-based graphite fibres exhibit a surface-oriented skin, although surface roughness increases with fibre modulus. The fibres all exhibit similar apparent surface energy characteristics which suggests that wettability does not play a significant role in determining interfacial bond strengths.

INTRODUCTION

The role of the fibre-matrix interface in determining overall composite mechanical properties is incompletely understood, not only in advanced composites containing high performance fibres such as boron and graphite,[1–3] but also in the more established glass fibre reinforced plastics.[3,4] However, there appears to be an incompatibility between the good interface adhesive bond required for maximum stress transfer to the fibres to achieve the best

†Presented at the Symposium on "Interfacial Bonding and Fracture in Polymeric, Metallic and Ceramic Composites" at the University of California at Los Angeles, Nov. 13–15, 1972. This Symposium was jointly sponsored by the Polymer Group of So. California Section, ACS and Materials Science Department, UCLA.

composite mechanical properties and some form of energy absorbing interface interaction needed for high fracture toughness.[5,6] There is thus a need to know the basic factors involved in interfacial adhesion in fibre reinforced materials and to be able to control them.

With graphite fibre composites, most effort has been concentrated on increasing composite mechanical properties, especially interlaminar shear whose early values were low compared with glass and boron fibre composites. Believed due to poor fibre-matrix adhesion, this situation has to a large extent been remedied by application of various fibre surface treatments which ostensibly increase the interfacial bonding.[1,2,7] Unfortunately, this is often at the expense of some fibre strength or modulus degradation.[1,8] The effects on interface adhesion and/or composite properties produced by these various surface treatments on the graphite fibres are often inconsistent and are, as yet, poorly understood.[1] Two main reasons for this are firstly, the insensitivity associated with using bulk composite properties for assessing interface interactions,[6,9] especially interlaminar shear as measured by the short beam shear test.[8,10] Secondly, there is usually an incomplete knowledge of fibre surface characteristics such as microstructure and chemical functionality and a lack of fibre surface energy data.

This paper presents the results of an attempt to make a direct measurement of fibre–matrix interface adhesion between graphite fibres and an epoxy matrix. In addition, some aspects of the surface characteristics of the particular fibres used are discussed in relation to the adhesion results.

A single filament model composite test method has been used to measure directly the tensile and shear strengths of interfacial bonding between resin matrices and large diameter ($>100\mu m$) glass and boron fibres,[4] but not for the smaller diameter ($<10\mu m$) carbon and graphite fibres so far available. The development of larger diameter (20–50μm), high performance, graphite fibres from pitch precursor in this laboratory has allowed application of this particular test method to the study of interfacial phenomena of these fibres.

EXPERIMENTAL

A) Materials

The large diameter high performance graphite fibres are prepared by strain graphitisation of thick glassy carbon fibres derived from pitch precursor.[11] Figure 1 shows examples of the size and shape of filaments which can be obtained by this route compared with the usual carbon and graphite fibres available commercially. The structure and properties of the present fibres depend mainly on the extent of elongation imposed upon them during the

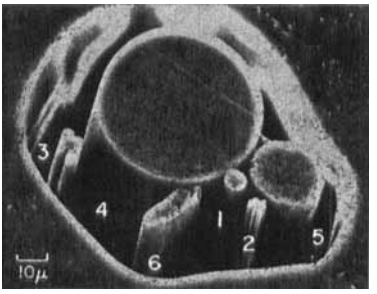

FIGURE 1 Cross sections of pitch-based carbon and graphite filaments compared with those available commercially. (1) Modmor I Fibre, (2) Thornel 50 Fibre, (3) Fortafil 5–T Fibre, (4) C.M.R. Glassy Carbon Fibre, (5) C.M.R. Graphite Fibre ($E \sim 60 \times 10^6$ p.s.i.), (6) C.M.R. Graphite Microtape ($E \sim 50 \times 10^6$ p.s.i.).

high temperature deformation process.[12] A wide spectrum of fibre properties is thus available ranging from those characteristic of an isotropic to those of a very highly oriented graphite fibre structure.

For the present experiments, fibres visibly free from defects were selected, cleaned with trichlorethylene and dried at 100°C. Boron fibres were similarly treated and glass fibres were freshly drawn from Pyrex rods.

The resin matrix chosen for use in the model composites was the room temperature curing epoxy system EPON 828/10 p.h.r. diethylenetriamine.

Glassy carbon plates were obtained from Beckwith Carbon Corp. and Polycarbon Inc., while sample pieces of stress-annealed pyrolytic graphite (SAPG) were obtained from Union Carbide Corp. Reagent grade liquids were used for contact angle measurements.

B) Specimen preparation

Tensile debond model composite specimens were molded in an aluminium split mold to give samples as in Figure 2a. Considerable care was exercised to ensure that no surface contamination of the fibres occurred during handling and that they were mounted straight. Shear debond specimens with the geometry shown in Figure 2b were prepared in individual molds as described in Ref. 4. Fibre length was $\frac{1}{3}$ that of the sample whose length-to-width ratio was 3:1.

For each molding, resin and curing agent were mixed and degassed under vacuum for standard times of 6 mins. and 3 mins. respectively. The resin was cured in the molds for 16 hours and a further 24 hours out of the mold. Subsequent to preparation of individual specimens by cutting and/or polishing, they were inspected for fibre alignment, interface integrity, etc. before selection for testing.

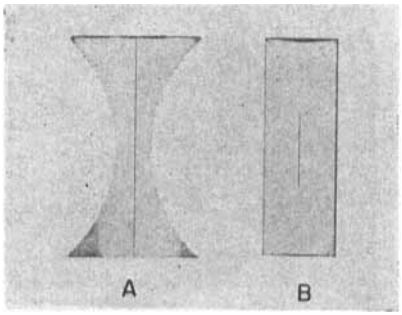

FIGURE 2 Model Composite Test Specimens (A) Tensile Debond Sample, (B) Shear Debond Sample.

C) Debond testing

Samples were tested by compressive loading in an Instron machine at 0.02″/min. crosshead speed. Throughout the test, the fibre-matrix interface was observed visually under suitable (dark field) illumination. The load on the sample was recorded when a sudden brightening of the light reflected from the interface was observed at the sample neck or fibre ends respectively for the tensile and shear debonding mode specimens. For the curved neck samples, a 10X, long-focus telescope was used at first, but it became necessary to use higher magnification (70X). For reasons described below, concurrent observation of the fibre at high magnification in transmission was also made during testing. Both ends of the fibre were observed with reflected light at high magnification during compression of the shear debond test specimens.

D) Fibre surface characterisation

Fibre surface topography has been investigated by scanning and replica electron microscopy. Microstructural features of the range of graphite fibres was studied by examination of the filament cross-sections under polarised light.[13] A goniometric technique[14] using the level surface principle was adopted to measure water contact angles on the fibres. Surfaces of highly polished bulk glassy carbon and cleaved basal surfaces of SAPG were used as models of fibre surfaces. The wettability of these were assessed by measuring the contact angles exhibited by a number of liquids of different surface tension on the surfaces, using the sessile drop and tilting plate methods. Liquid surface tensions were measured with a de Nouy balance. Where significant differences from literature values were obtained, the liquid was purified by distillation and the surface tension remeasured.

RESULTS AND DISCUSSION

A) Model composite testing—tensile mode

In the case of boron and glass fibres, axial compression of the model composites with curved neck geometry leads to interface tensile failure (debond). The greater Poisson's ratio of the resin over that of the fibre causes a net radial tensile force in the resin to operate away from the fibre surface. Interface separation is observed optically as a sharply increased reflectivity of the surface[4] at the sample neck. Preliminary testing of similar samples with the present graphite fibres indicated that, although more difficult to observe than with glass or boron, fibre surface reflectivity also increased at some particular compression load. The visual change was easiest defined for the lower modulus graphite fibres, but did not always seem to initiate at the sample neck. Subsequent testing of the range of fibres produced a scattered but reasonably monotonic progression in the axial stress values at the observed interface event from ~16,000 p.s.i. to ~6,000 p.s.i., decreasing the more highly oriented the fibres. Boron fibres were incorporated as controls.

After the testing of some graphite fibres which had been oxidised in nitric acid solution and which gave no change in "debond" test results, some large graphite microtape samples were molded to permit easier visual observation of the interface during testing. Many small highly reflecting areas were observed to appear at the instant of "debond" rather than a single area. High magnification optical examination of polished-down samples showed the presence of multiple cracks and fractures on the microtape and inspection of previously tested samples showed that all graphite fibres were similarly fractured. As can be seen in Figure 3, on either side of the compression induced failure the fibre exhibits a much more highly reflecting surface where the interface has been disturbed. Further "debond" tests observing the fibres

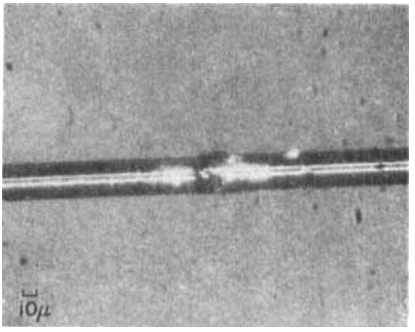

FIGURE 3 Highly reflecting interface appears on either side of fibre fracture in Tensile Debond sample.

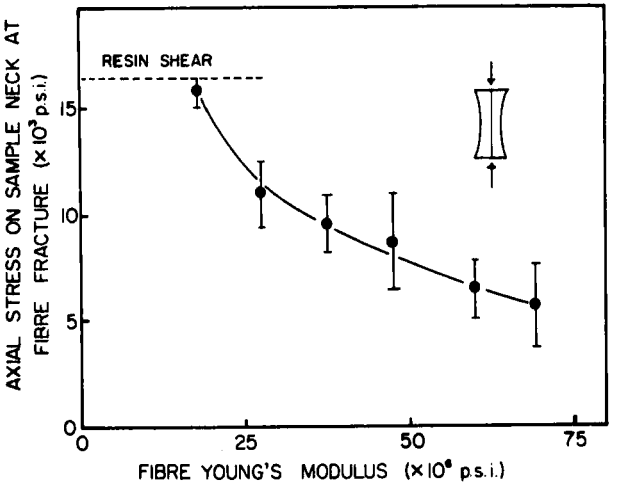

FIGURE 4 Variation of the axial stress on sample neck at instant of fibre fracture during sample compression with fibre Young's modulus.

under high magnification (70X) during sample compression confirmed that the event associated with sudden interface brightening was indeed fibre fracture with accompanying interface disruption rather than a true tensile failure of the fibre–resin interface. The results of the compression tests for the range of graphite fibres are shown in Figure 4. Each point represents the mean of 10–15 individual tests; error bars indicate range of results.

Fibre fractures are characteristic of a compression induced shear failure and are apparent first as fine circumferential cracks (Figure 5), which upon further axial compression produce a separation and eventual overlap of the sheared fibre ends. Identical failures were also observed in PAN and rayon–

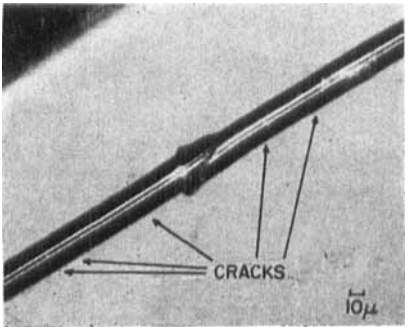

FIGURE 5 Compression shear fracture and circumferential cracking which precedes fracture of graphite fibre in tensile debond sample under compression.

based fibres when similarly tested in the curved-neck samples and no tensile interface debond was obtained. Samples molded with very large diameter, pyrolytic carbon/boron alloy fibres (Hough/NASA) also fractured without debond just after resin shear failure. The large elastic energy released on fibre fracture caused the resin to shatter around the break as shown in Figure 6 and was clearly audible.

According to Broutman[4] when interfacial tensile debond occurs in the curved-neck sample under elastic deformation conditions, the debond stress, S, is given by the equation

$$S = \frac{\sigma_m(\nu_m - \nu_f)E_f}{(1 + \nu_m)E_f + (1 - \nu_f - \nu_f^2)E_m} \tag{1}$$

where σ_m = axial stress on minimum section
ν = Poisson's ratio
E = Young's modulus and

subscripts f and m refer to fibre and matrix. Since $E_m \ll E_f$ even for the lowest modulus graphite fibres, this expression can be simplified to

$$S = \left(\frac{\nu_m - \nu_f}{1 + \nu_m}\right)\sigma_m \tag{2}$$

where the bracketed term may be considered as a stress concentrating factor. Where interface debond occurs after appreciable inelastic deformation of the sample, e.g. after yield, then an energy parameter may be a more appropriate measure of adhesion.[15]

Since in the testing of specimens with the present graphite fibres, no true interface debond occurred before fibre fracture (which usually occurred in the elastic portion of the stress–strain curve), the curve in Figure 4 serves to define minimum values for debonding. Figure 7 presents calculated minimum interface tensile bond strengths based on the mean data of Figure 4. ν_m for

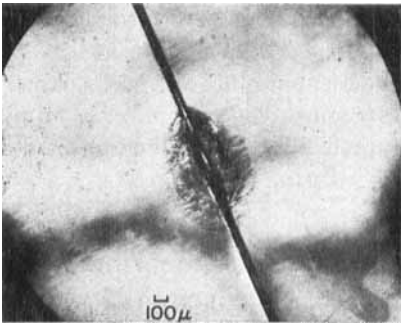

FIGURE 6 Compression fracture of pyrolytic graphite–boron alloy fibre and accompanying resin failure zone.

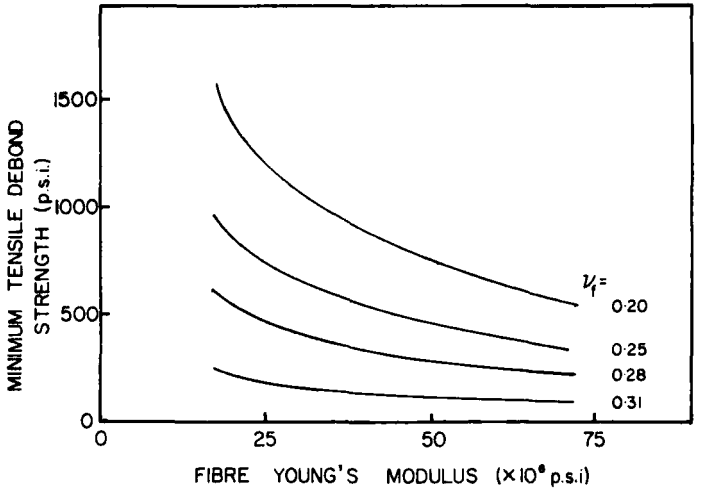

FIGURE 7 Minimum tensile debond strengths calculated from debond test results as a function of fibre Young's modulus.

the cured epoxy resin was determined as 0.33. Poisson's ratios have not been directly measured for any type of carbon or graphite fibre and literature values derived either theoretically or from composite data vary widely, between about 0.15 and 0.4. It is reasonable to suppose that values close to 0.28, that of bulk glassy carbon whose structure is identical to the isotropic graphite fibre, are most appropriate.

In comparing these results on graphite fibres with previous data on glass and boron fibres listed in Table I, it should be recalled that the present epoxy resin was cured at room temperature. Only a small exotherm (8° maximum) was measured in the small mold volume. Therefore, little residual compressive interface stress due to thermal coefficient differences contribute to these minimum bond strengths, although cure shrinkage will still contribute. Such thermally induced stresses have been estimated at up to 1000 p.s.i. for elevated temperature cured model composites with glass fibres.[16] Thus, although the tensile debond test does not provide quantitative results, it does suggest that the strength of the graphite fibre–epoxy bonding should be of a similar order to that measured for boron and glass fibres.

B) Model composite testing—shear mode

The model composite specimen as shown in Figure 2b, a rectangular block of resin containing a single fibre centrally embedded, is designed to induce interface shear debonding upon axial compression of the sample.[4]

TABLE I
Interface bond strengths measured by single fibre–resin tensile debond tests

Fibre	Resin (curing agent)	Cure temp. (°C)	Tensile strength (p.s.i.)	Reference
Glass	Polyester	50	> 1100	Calculated from data of ref. 15
Glass	Polyester	49	750–1200	4
Glass	Polyester	?	870–1450	21
Glass (toluene cleaned)	Epoxy (D.E.T.A.)	38	> 1540	4
Glass	Epoxy (D.E.T.A.)	?	1570	22
Glass	Epoxy (D.E.T.A.)	R.T.	> 1400	This work
Boron	Epoxy (MPD)	65	830	4
Boron	Epoxy (MNA/BDMA)	100	850–1630	23
Boron	Epoxy (D.E.T.A.)	R.T.	760	This work

For the present series of graphite fibres, genuine shear failure was observed, but fibre compression fracture was also found to occur and predominated for the highest oriented fibres. The results of compression tests on the shear debond specimens containing the various pitch-based graphite fibres are shown in Figure 8, where plotted points are mean values of at least 10 individual tests. (Some results are included for high modulus Thornel fibres; fracture in these was much more difficult to observe during testing.)

With the lowest modulus fibres, interface failure first initiated at the fibre ends followed at a higher stress by a sudden propagation along the fibre towards the specimen centre (Region A in Figure 8). Failure was not simultaneous at both ends, but the failure characteristics were similar. In many cases a progressive, slow or intermittent growth of the debonded interface occurred between initiation and propagation steps, similar to what has been observed with boron[4] and recently, glass specimens.[17] For fibres of Young's modulus $\sim 25 \times 10^6$ p.s.i., it was usually not possible to discern a sudden jump in the length of the highly reflecting region, the process after initiation appearing as a continuous unzipping of the interface until the entire fibre was debonded (Region B). With still higher modulus fibres, initiation was followed by compression fracture of the fibre, when the strain induced in the filament by interfacial stress transfer exceeded its ultimate compression fracture strain. Once this took place, shear stress was relieved at the interface and no debond propagation was observed thereafter (Region C). A fibre where debond initiated then progressed slowly, followed by fibre fracture is illustrated in Figure 9. Fibres of Young's modulus $\gtrsim 50 \times 10^6$ p.s.i. fractured even before debond initiated and thus precluded any subsequent interface failure (Region D).

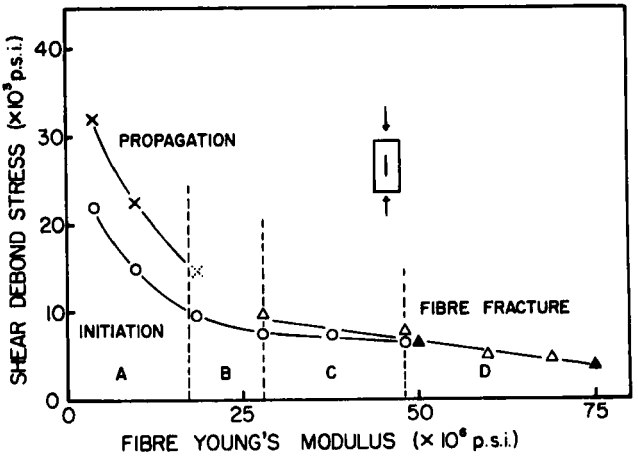

FIGURE 8 Variation of shear debond stress for graphite fibres with fibre Young's modulus. Areas A, B, C and D indicate approximate bounds of different failure regimes as described in the text. ○ Initiation, × Propagation, △ Fracture, Pitch-based Fibres; ▲ Fracture, Thornel Fibres.

The stress state around the tip of a single fibre embedded in a matrix which is being deformed is complex and the exact stress concentrating factor somewhat uncertain.[4,18] Broutman[4] considered that to a reasonable approximation the maximum shear stress, τ, at the end of a fibre of undefined shape is given by the expression

$$\tau = 2.5\,\sigma_{av.} \tag{3}$$

where $\sigma_{av.}$ is the average axial stress at debond for both fibre ends. The initiation and propagation debond values of Figure 8 were both calculated using Eq. 3, although originally it was applied to the propagation step only,

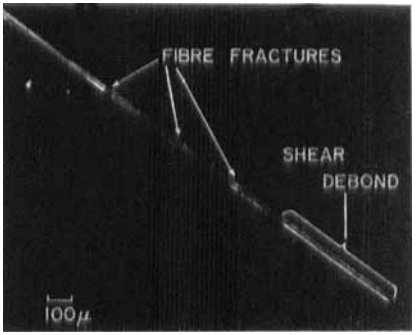

FIGURE 9 Shear debonded zone and fibre compression fractures in a graphite fibre-epoxy resin shear debond sample (Fibre Modulus $\sim 45 \times 10^6$ p.s.i.).

which was taken as the debond failure criterion.[4] This seems reasonable since variable geometric end effects are thus minimised. On the other hand, the stress to initiate debonding has been used to evaluate the relative adhesive behavior of size-coated glass fibres in polyester resins.[17] Whichever value is taken as a measure of interface adhesion in the present case, it is clear that a similar progression from high to lower bond strength is obtained from the isotropic to the oriented graphite fibres. (Fracture stress for fibres of modulus $\gtrsim 50 \times 10^6$ p.s.i. defines a minimum shear debond strength).

Presently measured shear debond strengths for glass and boron fibres agree reasonably well with published data and these together with results obtained for glassy carbon and graphite/boron alloy fibres are collected in Table II for comparison with the graphite fibre values. The shear debond strengths of the graphite fibres are similar to or greater than (depending on modulus) the boron and glass fibre results, suggesting good adhesion to epoxy resins; the glassy carbon value is also high. In most cases, the interface shear debond strengths exceed the yield strength of the resin in shear.

It is well extablished that interlaminar shear strength (I.L.S.S.) measurements on composites with intermediate and high modulus carbon and graphite fibres (untreated, commercial fibres) at 2000–5000 p.s.i. are considerably lower than those of glass and boron.[1,5] Only with low modulus carbon yarns have values of I.L.S.S. been obtained above 10,000 p.s.i.[19] A strict comparison cannot be made between I.L.S.S. and present debond results as there are no

TABLE II

Interface bond strengths measured by single fibre–resin shear debond tests

Fibre	Resin (curing agent)	Cure temp. (°C)	Shear	Shear strength (p.s.i.)	Reference
Boron	Epoxy (M.P.D.)	85	P	~ 7500	Quoted in 4
Boron (hot methanol wash)	Epoxy (M.P.D.)	85	P	~ 2800	Quoted in 4
Boron	Epoxy (D.E.T.A.)	R.T.	I	3140	This work
			P	3970	This work
Glass	Polyester	R.T.	I	3200– 9400[a]	17
			P	7000–13,200[a]	17
Glass	Epoxy (D.E.T.A.)	R.T.	I	4910	This work
			P	10,050	This work
Glassy carbon	Epoxy (D.E.T.A.)	R.T.	I	22,880	This work
			P	32,000	This work
Graphite/boron alloy[b]	Epoxy (D.E.T.A.)	R.T.	I	8750	This work
			P	15,820	This work

I refers to initiation of debond at fibre end.
P refers to rapid propagation of debond.
[a] Range of results depending on size treatment applied to glass fibre.
[b] Hough/NASA fibre.

I.L.S.S. data on pitch-based graphite fibres. However, the minimum shear debond strength obtained for Thornel 50 fibres compared to the corresponding ~2000 p.s.i. for I.L.S.S. does suggest that present debond shear strengths of the graphite fibres are rather high. A discrepancy between the I.L.S.S. data and both present and published debond results for boron fibres is also noted, although here the latter are low in comparison to I.L.S.S. figures. Results from both test methods for glass fibres are quite similar if the propagation step in the debond test is taken as the measure of interface adhesion.

There are, of course, differences between the stress states under load around a single fibre embedded in a matrix and the close-packed fibres in a practical composite, especially for stresses normal to the fibre axis.[18] Such differences could possibly lead to interface failure at lower axial stress in the model composite since, unlike the close-packed case, the effect of residual normal stresses due to curing would be additive to that induced upon sample compression. However, both residual and test induced normal interface stresses are smaller than shear stresses[16,18] and it is unlikely that such considerations will have significant effects on test results.

Both I.L.S.S. measurements and debond tests purport to measure the strength of fibre-matrix interfacial adhesive bonding. The discrepancies between the results of these two methods for the graphite and boron fibres might be reconciled if the stress concentrating factor of Eq. 3 varied with fibre type. This is not unreasonable in view of the critical dependence of the stress concentration on fibre end geometry[4,18] and the different physical structure (and fracture characteristics) of the different types of fibre. Experimental results would then suggest appropriate stress concentrating factors somewhat lower (for graphite) and higher (for boron) than the average value of 2.5 adopted by Broutman.[4]

Recently interface shear strengths of fibre–resin bonds have been measured by pull-out of fibres from a thin disc of epoxy resin.[20] For untreated fibres, results ranged from ~150 p.s.i. for high modulus (Type I) to ~1400 p.s.i. for intermediate modulus (Type II) PAN-based fibres and ~1200 p.s.i. for glassy carbon fibres prepared in this laboratory (C.M.R. fibres). Although much lower still than corresponding I.L.S.S. data, these results emphasize the high value of present shear debond results on carbon and graphite fibres. Pull-out shear adhesion strengths on glass fibres (quoted in Ref. 20b) at 4200–5500 p.s.i. are about half the value of corresponding I.L.S.S. data and as such are close to the debond initiation results of the shear debond test. It is obvious that further experiments are necessary to compare directly the several test methods for determining fibre–matrix adhesion with the same fibres before clarification of the meaning of results can be obtained.

C) Fibre surface characterisation

Whatever the significance of the absolute values of the interface debonding results, a progression in relative values is obtained for the series of graphite fibres. Provided bond failure does in fact take place at the interface then measured adhesion should be related to the nature of the fibre surfaces. The fibre physical topography may be of importance since it determines surface area available for bonding and surface roughness may provide for some mechanical keying. The surface microstructure should influence adhesion through its effect on chemical reactivity, functionality and surface energy characteristics. The surface chemical nature of present fibres has not been studied, but topography and microstructure have and attempts to assess fibre wettability and surface energy parameters have been made.

The large range of structure exhibited by the pitch-based fibres extends from the unstretched, isotropic to the highly oriented where the graphite basal planes are aligned preferentially along the fibre axis. These filaments have essentially the same bulk property and microstructural features as the textile polymer-based fibres at equivalent Young's modulus.[12] The series of replica electron micrographs of Figure 10 shows clearly an increasing surface roughness from low to high modulus fibres. The increasing axial rilled surface nature is a reflection of the progressive change in microstructure from the glassy to the fibrillar texture with accompanying diametral shrinkage of the fibres upon axial stretching during their fabrication.[12,24] This increase in roughness is in the opposite direction to the interfacial adhesion results of the debond tests and suggests that mechanical keying and apparent gross surface area do not play a major role in determining bond strength. The increasing roughness along the series may exert an influence on debond results by increasing the severity of stress concentrations.

Polarised light microscopy of polished fibre cross-sections indicates that the graphite fibres exhibit axial symmetry. Extinction crosses remain parallel to the crossed polarisers when specimens are rotated as in Figure 11a and b, indicating a degree of basal plane edge stacking about the fibre axis.[13] The extinction patterns shown by cross-sections of graphite microtapes, Figure 11c and d, indicate that the basal planes of a surface layer are aligned parallel to their surface and this is likely the case also for the cylindrical fibres. Such surface oriented layers are well established on PAN- and rayon-based fibres.[13,25] The detailed surface microstructure of the pitch-based graphite fibres is therefore similar to that of the others and they thus possess more "basal plane content" on their surfaces than might otherwise be expected.

The virgin surfaces of conventional carbon and graphite fibres exhibit slight polar chemical functionality, due mainly to groups such as carboxyl, hydroxyl and carbonyl,[1,2,7] thought to arise from environmental exposure.

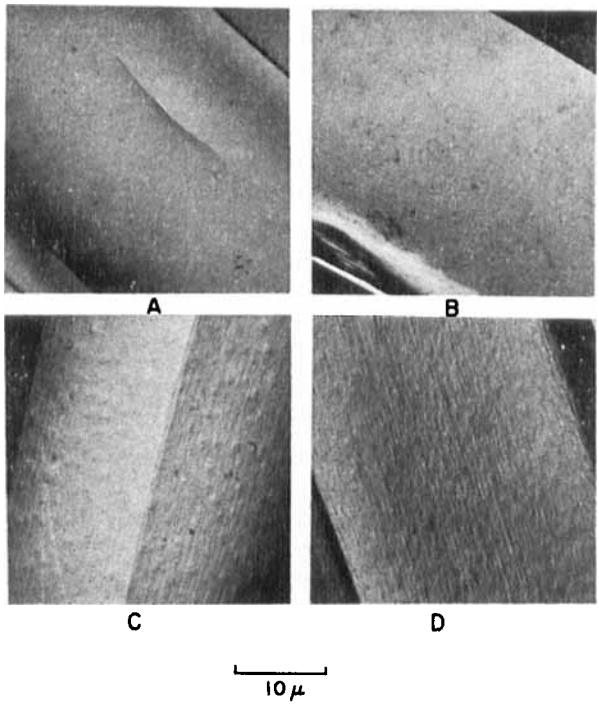

FIGURE 10 Replica electron micrographs of the surfaces of pitch-based graphite fibres. (A) Unstretched graphite (E $\sim 4 \times 10^6$ p.s.i.), (B) Strain graphitised ($E \sim 25 \times 10^6$ p.s.i.), (C) Strain graphitised ($E \sim 50 \times 10^6$ p.s.i.), (D) Strain graphitised ($E \sim 80 \times 10^6$ p.s.i.).

Other elements which have been detected on untreated carbon fibre surfaces, e.g. N[2] and P, S and Cl[26] on PAN-based fibres and S on rayon-based fibres[27] remain from their precursors. Oxygen-containing groups probably also exist on present fibres, but it has been shown elsewhere[28] that they are relatively uncontaminated with other elements compared to type II PAN (carbon) fibres, but similar to the higher heat-treated type I (graphite) fibres. Thus, whatever contribution is made to adhesive bonding with epoxy resins by the surface chemical composition, it is likely to be similar for the corresponding untreated graphite fibres derived from the different precursors.

The structural features and chemical nature of graphite fibre surfaces should determine their surface energy and wettability characteristics. Adequate wetting is a necessary prerequisite for good adhesion, since it provides for intimate contact of substrate and liquid adhesive over the maximum interfacial area. These aspects of carbon and graphite fibre surfaces have not yet been adequately described, although the finite contact angles found for

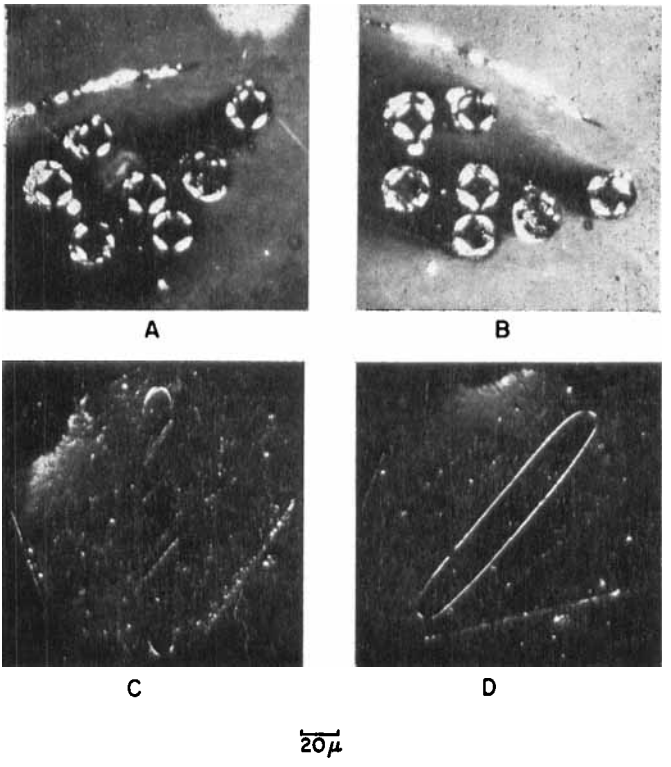

FIGURE 11 Polarised light optical micrographs of transverse sections of pitch-based graphite filaments showing orientation parallel to filament surface. (Polariser and analyser are parallel to picture edges.) (A) Graphite Fibre ($E \sim 50 \times 10^6$ p.s.i.), (B) As for A, but rotated ~45 C.W., (C) Graphite Microtape ($E \sim 20 \times 10^6$ p.s.i.), (D) As for C, but rotated ~45° C.W.

epoxy resins (and other liquids) on these fibres suggest that they exhibit low energy surfaces.[2,19] Contact angles of about 30° with epoxy are noted for the graphite fibres studied here.

From data on wicking of water into fibre bundles, Chwastiak[29] calculated contact angles which apparently indicated different surface characteristics on various carbon and graphite filaments. Results of water contact angles measured on the present graphite fibres using the level surface technique[14] are shown in Figure 12. Essentially a constant value was obtained for all fibres and only upon fibre oxidation was a variation along the series detected. These results prompted further investigation of the untreated filament surfaces.

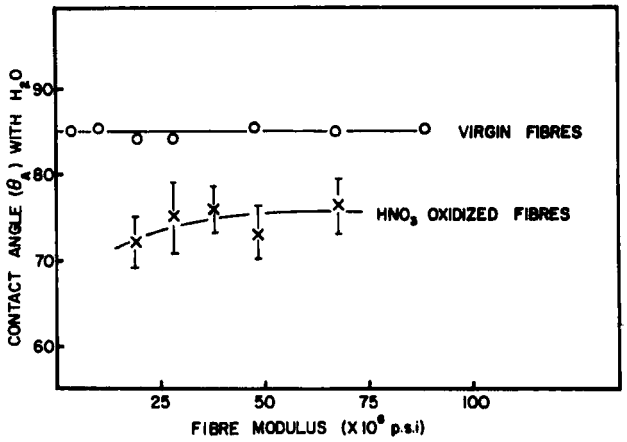

FIGURE 12 Advancing contact angle measured with water on pitch-based graphite fibres of various Young's modulus (using the level surface technique described in reference 14).

For solid surfaces in air, the appropriate parameter describing their surface energy state is the solid–vapour surface tension γ_{SV} which, however, cannot be measured directly. A useful approximation to γ_{SV}, widely used to characterise surface wettability, is Zisman's empirical parameter—the critical surface tension for wetting γ_c.[30] To determine γ_c over the range of present graphite fibres measurement of contact angles exhibited by several liquids of differing surface tension on three fibres was attempted. Reproducible angles were measured with increased difficulty the lower the angle and those below about 35° could not be satisfactorily established. The results, listed in Table III, show that no significant difference between fibres was detected. An approximate derived value for γ_c at 38 dyne cm. for all fibres is somewhat lower than a corresponding result obtained on other

TABLE III
Contact angles exhibited on three graphite fibres by various liquids

		Contact angle (θ_A)		
		Fibre 1	Fibre 2	Fibre 3
Liquid	γ_{LV} dynes cm.	($E \sim 5 \times 10^6$ p.s.i.)	($E \sim 28 \times 10^6$ p.s.i.)	($E \sim 60 \times 10^6$ p.s.i.)
Water	72	85 ± 1	84 ± 2	85 ± 2
Glycerol	63.5	74 ± 2	—	73 ± 2
Formamide	58	65 ± 2	62 ± 3	64 ± 3
Methylene iodide	51	39 ± 5	38 ± 5	37 ± 6
Ethylene glycol	48.5	53 ± 3	51 ± 3	53 ± 3

graphite fibres.[19] However, the present value is consistent with the observation of non-zero contact angles on the pitch-based graphite fibres exhibited by epoxy resin ($\gamma_{LV} = 45$ dyne cm.). Table IV lists known wettability and contact angle data on various carbon and graphite substrates for comparison with present graphite fibre results.

Because of the surprisingly constant surface wettability data and the experimental uncertainty of the fibre contact angle results, further evidence was considered desirable. Accordingly, the wettability of the surface of bulk glassy carbon and the cleaved basal plane surface of stress annealed pyrolytic graphite was determined. These model surfaces represent the two extremes of microstructures likely to be exhibited by the present series of graphite fibres. Contact angle results with a series of liquids (including those in Table III) obtained by two methods are shown plotted in Figure 13. The large scatter on the $\cos\theta - \gamma_{LV}$ field seems to be real in view of the agreement between results of the two techniques and probably arises from the fact that the liquids used are not in a homologous series[30] so that different intermolecular interactions with the substrates are involved.[31] Most interesting, however, is the agreement between results for the two different surfaces. The mean intercept at $\cos\theta = 1$ of the rectilinear band enclosing the results gives $\gamma_c = 37 \pm 7$ dyne cm. which agrees well with the fibre results. Contact angles of epoxy resin and resin with 10 p.h.r. DETA on these surfaces,

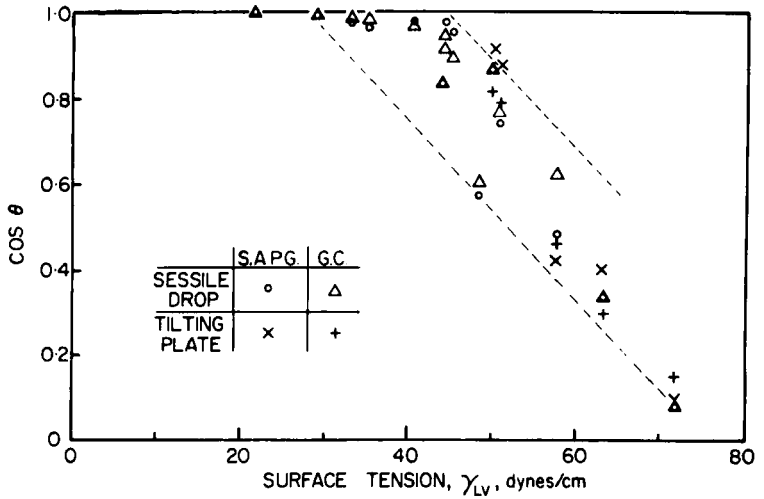

FIGURE 13 Cosine of the contact angle exhibited by a range of liquids of different surface tension on the surfaces of cleaved stress annealed pyrolytic graphite (S.A.P.G.) and polished glassy carbon (G.C.) measured by two different methods. (Maximum reproducible static contact angle used in sessile drop measurements, Reference 35.)

TABLE IV
Contact angle and wettability data on various carbons and graphites

Fibre/solid (treatment)	Method	Contact angle		γ_c	Ref.
		Water	Epoxy (type)		
Thornel 25	Photomicrograph	36	32 (ERLA 2774)		Quoted in 2
Thornel 25 (air oxidised)	Photomicrograph	38 ± 8	5.4 (ERLA 2774)		Quoted in 2
Thornel 25				46	19
Thornel 50 (H_2O sized)	Sink-float			25.7–22.9	2
Thornel 50	Dynamic wicking	≥90			29
Thornel 50 (PVA sized)	Dynamic wicking	40			29
Thornel 50 (oxidised)	Dynamic wicking	15–41			29
Modmor I	Dynamic wicking	≥90			29
Modmor II	Dynamic wicking	32			29
Modmor II (treated)	Dynamic wicking	28			29
Thermolon SM	Tilting fibre		72 (MY 750/		33
Thermolon ST	Tilting fibre		69 MNA/		33
Modmor I (treated)	Tilting fibre		65 BDMA)		33
Modmor II (treated)	Tilting fibre		62		33
Glassy carbon	Level surface	81 ± 3			This work
PG/boron alloy	Level surface	80 ± 2			This work
Graphitised Carbon black (pelletised)		82			34
Ceylon graphite (polished)	Tilting plate	85.6 ± 0.3			35
Pyrolytic carbon film				45 ± 2	1
Pyrolytic graphite—basal	Sessile drop		62 (ERLA 2256)		13
Pyrolytic graphite—edge	Sessile drop		48 (ERLA 2256)		13
SAPG—basal	Sessile drop	85.5 ± 0.5	33 ± 1 (EPON 828)	37 ± 7	This work
SAPG—edge (polished)	Sessile drop	85 ± 1	Wicking (EPON 828)		This work
Glassy carbon (polished)	Sessile drop	83 ± 2	33 ± 1 (EPON 828)	37 ± 7	This work

measured at 33° and 22° ± 1° respectively, confirm the lack of complete wetting and the constant results with the graphite fibres.

It appears therefore that no variation in surface energetics is detectable along the series of graphite fibres by the contact angle techniques used, contrary to expectations. Average surface conditions are monitored by

wettability methods and it is possible that such techniques are not sufficiently sensitive to detect what would have to be small differences in surface reactivity along the series of fibres with surface oriented layers. Oriented layers cannot be detected even in bulk glassy carbon heat-treated to graphitising temperatures. In view of this and the similarity of wettability data on this substrate to the fibres and SAPG, a more likely explanation is that under ambient conditions the presence of an absorbed layer of water or other contaminant[2] on all such surfaces masks any underlying variations in surface reactivity.

The nature of the controlling influence on fibre–matrix adhesion for the series of pitch-based graphite fibres still remains to be established as, indeed, does the precise locus of debond failure. If chemical bond formation is involved in the adhesion and true interface failure occurs then fibre surface energy and reactivity must be important. Assessment of the reactivity of other carbon and graphite fibres has been attempted by chromatographic techniques, but with little success so far.[2,7] Raman spectroscopy has proved useful in characterising carbon and graphite surfaces in terms of an "amount of crystal boundary".[25] A loosely defined parameter related to degree of graphicity and the potential chemical functionality of fibre surfaces, this has been shown to relate to interlaminar shear strengths of the corresponding fibre composites.[25] It may be worthwhile to examine present fibres by such a technique.

Surface energies of solids as determined by thermodynamic methods such as wettability measurements often provide only a partial contribution to the total solid surface energy, whereas mechanical fracture methods can yield total energies.[32] The interface failure behavior observed in shear debond tests is similar to that in crack growth experiments in monolithic solids where crack initiation is followed by slow growth until, at a critical crack length, catastrophic failure occurs. This suggests that a valid approach to the study of interfacial phenomena in fibre–matrix systems may be to examine the possibility of carrying out such crack growth experiments on model interfaces.

CONCLUSIONS

1) The tensile debond test is not applicable to carbon or graphite fibres with epoxy resins, since the fibres cannot sustain the compression strains involved in the test.

2) Interfacial failure is observed in the shear debond test with graphite fibres of low and intermediate Young's modulus, but thereafter compression fracture again occurs.

3) In tests where fibre fracture occurs minimum interface bond strengths can be defined.

4) The shear debond test indicates a progression in relative interface adhesion strength for pitch-based graphite fibres, the strength decreasing the higher the fibre Young's modulus.

5) Pitch-based graphite fibres possess a surface oriented layer similar to textile-based fibres and they exhibit an increasing surface roughness the higher the fibre Young's modulus.

6) Surface energy and wettability characteristics appear to be constant along this series of graphite fibres.

7) Interfacial adhesion strength between the graphite fibres and an epoxy resin matrix does not appear to be related to the fibre wettability characteristics.

Acknowledgements

We thank Messrs. G. Fraser, R. Palylyk and G. Takacs for assistance with various parts of the experimental work. Thanks are also expressed to A. W. Moore (Union Carbide Corp.), K. Marnock (Polycarbon Inc.), D. A. Scola (United Aircraft), D. L. McDaniels (NASA/Lewis), and K. R. Linger (Harwell) for samples of S.A.P.G., glassy carbon, boron fibres, pyrolytic graphite/boron alloy fibres and PAN-based fibres respectively. The financial support of this work by the Defense Research Board of Canada is gratefully acknowledged.

References

1. D. W. McKee and V. J. Mimeault, G.E. Report #70–C–247, July 1970 (also published in Vol. 8, "Chem. and Phys. of Carbon" 1973).
2. D. A. Scola and C. S. Brooks, *J. Adhesion* **2**, 213 (1970).
3. *Symposium on Composite Materials: Testing and Design*, ASTM STP 460 (1969).
4. L. J. Broutman, *Interfaces in Composites*, ASTM STP 452, 27 (1969).
5. B. Harris, P. W. R. Beaumont and E. M. de Ferran, *J. Materials Sci.* **6**, 238 (1971).
6. R. L. McCullough, *Concepts of Fibre–Resin Composites* (Marcel Dekker, N.Y., 1971).
7. J. V. Larsen, 161st A.C.S. Mtg. (Org. Coatings and Plast. Chem.) Paper 61, Los Angeles, April 1971.
8. W. N. Reynolds and N. L. Hancox, *J. Phys. D. (Appl. Phys.)* **4**, 1747 (1971).
9. A. M. Lovelace, *Materials Research and Standards, MTRSA* **11** (5), 8 (1971).
10. N. L. Hancox, *J. Materials Sci.* **7**, 1030 (1972).
11. H. M. Hawthorne *et al.*, *Nature* **227**, 946 (1970).
12. H. M. Hawthorne, Proc. 1st International Carbon Fibres Conf., London, 1971 (Plastics and Polymers Conf. Supplement #5), p. 81.
13. B. L. Butler, Ph.D. Thesis, Rensselaer Polytechnic Institute, 1969.
14. T. H. Grindstaff, *Textile Research J.* **39** (10), 958 (1969).
15. G. Mozzo and R. Chabord, Proc. 23rd Ann. Tech. Conf. S.P.I., Paper 9–C, Feb. 1968.
16. L. J. Broutman and F. J. McGarry, *Mod. Plastics* **40** (1), 161 (1962).
17. J. B. Shortall and H. C. Yip, Faraday Special Discussion on Solid–Solid Interfaces, Paper 14, Nottingham, Sept. 1972.
18. A. S. Carrara and F. J. McGarry, *J. Composite Materials* **2** (2), 222 (1968).

19. J. C. Goan and S. P. Prosen, *Interfaces in Composites*, ASTM STP 452, 3 (1969).
20. J. P. Favre and J. Perrin, (a) *J. Materials Sci.* **7**, 1113 (1972). (b) *Rech. Aerosp.* #1, 52, Jan./Feb. 1971.
21. R. Rothwell and M. Arrington, *Nature Phys. Sci.* **223**, 163 (1971).
22. T. D. Schlabach and S. Klosowski, Proc. 19th Ann. Tech. Conf. S.P.I., Paper 11–C, (Feb. 1964).
23. Calculated from data supplied by D. A. Scola (United Aircraft Lab.) 1971.
24. H. M. Hawthorne, to be published.
25. F. Tuinstra and J. L. Koenig, *J. Composite Materials* **4**, 492 (1970).
26. G. L. Connell, *Nature* **230**, 377 (1971).
27. M. L. Lieberman and G. T. Noles, *J. Materials Science* **7**, 654 (1972).
28. R. F. Willis, B. Fitton and D. K. Skinner, *J. Appl. Phys.* **43** (11), 4412 (1972).
29. S. Chwastiak, A.C.S. Preprints (Org. Coatings and Plastics Chem.) **13** (1), 437 (1971).
30. W. A. Zisman in *Contact Angle, Wettability and Adhesion*, Advances in Chemistry Series 43 (A.C.S., Washington, 1964).
31. F. M. Fowkes in *Fundamental Phenomena in the Materials Sciences*, Vol. 2: *Surfaces*, Ed. L. J. Bonis and H. H. Hauser (Plenum Press, N.Y., 1965).
32. J. J. Duga, Surface Energy of Ceramic Materials, D.C.I.C. Report, 69–2, 1969.
33. M. Yamamoto, *et al.*, Proc. 1st International Carbon Fibres Conf., London, 1971, (Plastics & Polymers Conf. Suppl. 5), p. 179.
34. G. Y. Young, *et al.*, J.A.C.S. **58**, 313 (1954).
35. F. M. Fowkes and W. D. Harkins, *ibid* **42**, 3377 (1940).
36. H. W. Fox and W. A. Zisman, *J. Colloid Science* **5**, 514 (1950).